13th World Conference on Earthquake Engineering
Vancouver, B.C., Canada
August 1-6, 2004
Paper No. 1880

EXPERIMENTAL STUDY ON SEISMIC CAPACITY OF REINFORCED FULLY GROUNTED CONCRETE MASONRY WALLS

Kenji KIKUCHI[1], Koji YOSHIMURA[2], Kazuhiko YOSHIDA[3], Akihiro TANAKA[4]
Hirokuni URASAKI[5], Yohei KIJIMA[6] and Nobuaki MIZUMASA[7]

SUMMARY

Reinforced fully-grouted concrete masonry building system, which is one of the boxed-wall structures, is composed of grouted masonry walls, reinforced concrete (R/C) wall girders and floor slabs. In order to establish a better structural design method based on the seismic capacity for this type of masonry buildings, it is necessary to evaluate the seismic capacity of the grouted masonry walls subjected to severe earthquake loading quantitatively. Main objective of the present study is to investigate the seismic capacity of the wall experimentally. Herein, various kinds of grouted masonry wall specimens are tested under the conditions of different constant vertical axial loads and alternately repeated lateral forces. Main parameters adopted for the experiment are (1) the aspect ratio of the wall, which is related to shear span ratio, (2) vertical axial load, (3) amount of wall reinforcement, and (4) strengthening techniques for preventing the wall from sliding failure along the bottom joint of the wall panel. The test results indicate that a sliding strengthening by using dowel-reinforcing bars is effective to prevent the bearing walls from sliding failure and the ultimate flexural strengths of grouted masonry walls can be well predicted by the existing proposed equations. In addition, by improving the terms related to wall axial loads in the existing equations, the accuracy to predict the ultimate shear and sliding strengths has increased.

INTRODUCTION

Reinforced fully-grouted concrete masonry building system, which is one of the boxed-wall structures, is composed of grouted masonry walls, R/C wall girders and floor slabs as shown in Fig. 1. Fig. 2 shows an example of buildings using this structural system. This masonry building system is expected to be used more widely in the future in Japan, because there was almost no structural damage to this type of masonry

---

[1] Professor, Oita University, Japan. Email: kikuchi@cc.oita-u.ac.jp
[2] Professor, Oita University, Japan. Email: kojiysmr@cc.oita-u.ac.jp
[3] Lecturer, Oita Institute of Technology, Japan. Email: kyoshida@oita-it.ac.jp
[4] Structural Engineer, Umebayashi Corp., Japan. Email: a-tanaka@umebayashi.jp
[5] Structural Engineer, Kyuken Architects and Engineers Inc., Japan. Email: urasaki@kyuken.co.jp
[6] Graduate Student, Oita University, Japan, Email: youhei40@arch.oita-u.ac.jp
[7] Graduate Student, Oita University, Japan, Email: mizumasa@arch.oita-u.ac.jp

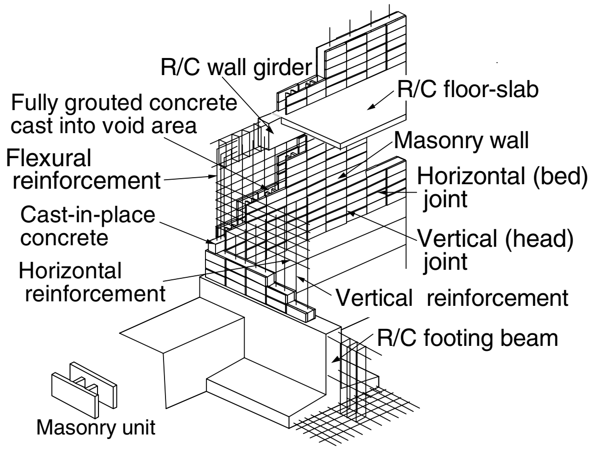

Fig. 1 Typical reinforced fully-grouted concrete masonry building system

Fig. 2 A reinforced fully-grouted concrete masonry building in Japan

buildings during the 1995 Hyogoken-nanbu (Kobe) earthquake (Bruneau [1]), and they have also excellent capacity in durability, fire resistance, sound insulation and so on.

This type of buildings have been designed according to the AIJ (Architectural Institute of Japan) Standard for Structural Design of Grouted Masonry Building Structures (AIJ [2]). This Standard is based on the allowable stress design method using the concept of "wall rate" values, a simple ratio expressed by the horizontal length of the bearing walls in each direction and in each story, divided by the total floor area of the story. This design method is simple and useful, but insufficient to evaluate the accurate seismic performance of a designed building. In order to establish the better structural design method based on the seismic performance for this type of masonry buildings, it is necessary to evaluate the seismic capacity of the grouted masonry walls subjected to severe earthquake loading quantitatively.

Main objective of the present study is to investigate the seismic capacity of the wall experimentally. A total of nineteen grouted masonry wall specimens were designed and constructed. Main experimental parameters adopted for the experiment are (1) aspect ratio of the wall, which is related to shear span ratio, (2) vertical axial load, (3) amount of wall reinforcement, and (4) strengthening method for preventing the wall from sliding failure along the bottom of the wall panel. All specimens were tested under the conditions of a constant vertical axial load and alternately repeated lateral forces.

TEST SPECIMENS

Nineteen different bearing wall specimens were designed and constructed and their details are listed in Table 1. Fig. 3 shows the size and shape, and the reinforcement of the typical test specimens. Size and shape of the hollow concrete masonry unit used for the grouted masonry walls is shown in Fig. 4. All the specimens are approximately two-third scale models of one-story bearing walls. Clear height (h_o) of the wall panel is 1200 mm, and the total height of the bearing wall is 1500 mm including the depth of the cast-in-place wall girders located at the top of each wall. The width of horizontal and vertical mortar joints in the grouted masonry walls is 6.7 mm. Four different aspect ratios (h_o/l), which are 0.75, 0.90, 1.13 and 1.51, are adopted for the wall panels of the specimens. In addition, all the nineteen specimens are classified into two test series, F- and S-series, depending on the amount of vertical and horizontal reinforcements. As shown in Table 1 and Fig. 3, wall panels in F-series specimens have one longitudinal flexural reinforcing bar (rebar) of 1-D16 in each of the wall edges, vertical rebars of D10 at 267 mm spacing, and horizontal rebars of D13 at 133 mm spacing. S-series specimens have also one longitudinal

Table 1 List of test specimens

Specimen		Clear Height of Wall h_0 (mm)	Wall Length l (mm)	Aspect Ratio h_0/l	Shear Span Ratio M/Ql	Flexural Rebar $\langle a_t$(mm^2)$\rangle$	Flexural Rebar p_t^{*1}(%)	Vertical Rebar a_{wv}	Horizontal Rebar a_{wh}	Horizontal Rebar p_{wh}^{*2} (%)	Dowel Rebar	Vertical Axial Load N(kN)	Vertical Axial Stress σ_0 (MPa)
F-series Specimens	FN-1.51L-LC	1200	793	1.51	0.83	1-D16 (#5) <199>	0.20	D10 (#3) @267	D13 (#4) @133	0.72	-	83	0.78
	FS-1.51L-LC										D13 (#4) @267		
	FN-1.13L-LC		1060	1.13	0.62		0.15				-	111	
	FS-1.13L-LC										D13 (#4) @267		
	FN-0.90L-LC		1326	0.90	0.50		0.12				-	138	
	FS-0.90L-LC										D16 (#5) @267 only the edges of wall:D13		
S-series Specimens	SN-1.51L-LC		793	1.51	0.83	1-D22 (#7) <387>	0.39		D10 (#3) @267	0.20	-	83	
	SN-1.13L-LC		1060	1.13	0.62		0.29				-	111	
	SN-0.90L-0		1326	0.90	0.50		0.23				-	0	0.00
	SN-0.90L-LC											138	0.78
	SN-0.90L-LC2												
	SN-0.90L-HC											313	1.77
	SS-0.90L-0										D16 (#5) @267 only the edges of wall:D13	0	0.00
	SS-0.90L-LC											138	0.78
	SS-0.90L-LC2												
	SN-0.75L-0		1593	0.75	0.41		0.19				-	0	0.00
	SN-0.75L-LC											166	0.78
	SN-0.75L-HC											373	1.77
	SS-0.75L-LC										D16 (#5) @267 only the edges of wall:D13	166	0.78

[Remarks] *1 p_t = flexural reinforcement ratio = a_t / tl,
where a_t = cross-sectional area of flexural rebars, l = wall length, t = wall thickness
*2 p_{wh} = shear reinforcement ratio in horizontal direction = a_{wh} / th_o,
where a_{wh} = cross-sectional area of all horizontal rebars, h_o = clear height of wall

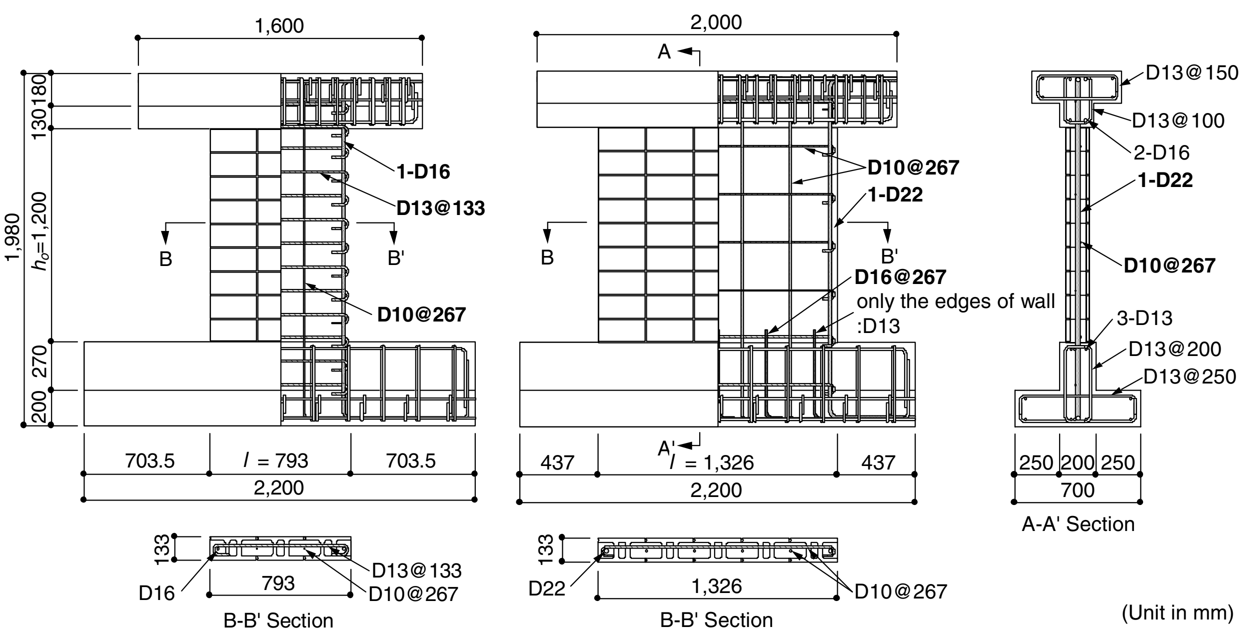

(a) FN-1.51L-LC **(b) SS-0.90L-LC**

Fig. 3 Size and shape, and reinforcement of test specimens

flexural rebar with bar-size of 1-D22 at each wall edge, and vertical and horizontal rebars with bar-size of D10 at 267 mm spacing.

Each of the specimens is designated by a four symbol code, such as (FN-1.51L-LC) and (SS-0.90L-LC). The first symbol “F” or “S” represents difference in the amount of vertical and horizontal reinforcement.

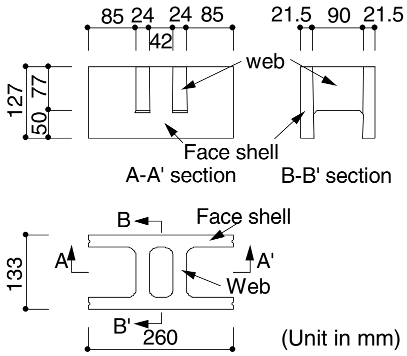

Fig. 4 Size and shape of masonry unit

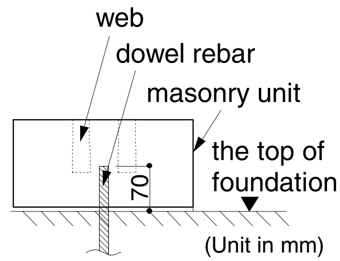

Fig. 5 Dowel rebar for sliding strengthening

Table 2 Mechanical properties of reinforcing bars

Specimens	Rebars	Yield Strength (MPa)	Tensile Strength (MPa)	Elongation (%)
FN-1.51L-LC FN-1.13L-LC FN-0.90L-LC SN-1.51L-LC SN-1.13L-LC SN-0.90L-LC	D22 (#7)	333	498	22
	D16 (#5)	345	518	22
	D13 (#4)	370	515	22
	D10 (#3)	339	483	20
FS-1.51L-LC FS-1.13L-LC FS-0.90L-LC SS-0.90L-LC	D22 (#7)	333	498	22
	D16 (#5)	345	518	22
	D13 (#4)	327	459	23
	D10 (#3)	339	483	20
SN-0.90L-0 SN-0.90L-LC2 SN-0.90L-HC SS-0.90L-0 SS-0.90L-LC2	D22 (#7)	332	493	26
	D16 (#5)	354	514	26
	D13 (#4)	352	497	27
	D10 (#3)	346	492	24
SN-0.75L-0 SN-0.75L-LC SN-0.75L-HC SS-0.75L-LC	D22 (#7)	339	514	27
	D16 (#5)	354	514	26
	D13 (#4)	332	497	27
	D10 (#3)	357	502	25

Table 3 Compressive strengths of concrete, mortar, masonry unit and prism

Specimens	Concrete (MPa)	Joint Mortar (MPa)	Masonry Unit (MPa) (per net section)	Prism (MPa)
FN-1.51L-LC	33.5	48.7	33.6	28.3
FN-1.13L-LC	32.2	43.7		26.5
FN-0.90L-LC	34.3	51.0		32.5
SN-1.51L-LC	32.7	49.2		27.2
SN-1.13L-LC	34.1	50.7		33.6
SN-0.90L-LC	27.3	47.1		30.2
FS-1.51L-LC	29.8	39.4	46.5	29.2
FS-1.13L-LC	33.9			32.1
FS-0.90L-LC	34.4			32.1
SS-0.90L-LC	38.9			34.6
SN-0.90L-0	32.4	34.4	50.5	27.9
SN-0.90L-LC2	38.3			26.6
SN-0.90L-HC	29.4			26.9
SS-0.90L-0	32.1			30.9
SS-0.90L-LC2	32.1			26.7
SN-0.75L-0	35.1	34.4	46.2	26.9
SN-0.75L-LC	36.1			26.9
SN-0.75L-HC	31.7			27.7
SS-0.75L-LC	32.9			27.2

The second symbol "S" represents the presence of dowel rebars, which are provided along the bottom of wall as shown in Fig. 5 in order to increase the sliding resistance of the wall-bottom, and "N" means that no dowel rebars are provided. The third symbol, "1.51L", "1.13L", "0.90L" or "0.75L" represents the aspect ratio of the wall. In the specimens with the aspect ratio of 1.51 or 1.13, the dowel rebars with bar-size of D13 are provided at 267 mm spacing. In the specimens with the aspect ratio of 0.90 or 0.75, the dowel rebars with bar-size of D16 are provided at 267 mm spacing, except that the dowel rebars of D13 were used at both wall edges. The fourth symbol, "0", "LC" or "HC" represents the constant vertical axial stresses of 0MPa, 0.78MPa or 1.77MPa are applied to the specimens, respectively. Mechanical properties of materials used for the specimens are shown in Tables 2 and 3, which are the average of at least three measurements.

TEST SETUP AND TEST PROCEDURE

The test setups adopted in the present study are shown in Figs. 6(a) and (b). The specimens were tested by using the test setup A, as shown in Fig. 6(a) except for the specimens with the wall aspect ratio of 0.75, which were tested by using the test setup B in Fig. 6(b). Constant vertical axial loads were applied by a hydraulic jack (V) and alternately repeated lateral forces were applied by a double-acting hydraulic jack (H). The height of the longitudinal axis of lateral forces applied to all the specimens is 0.55 times the clear

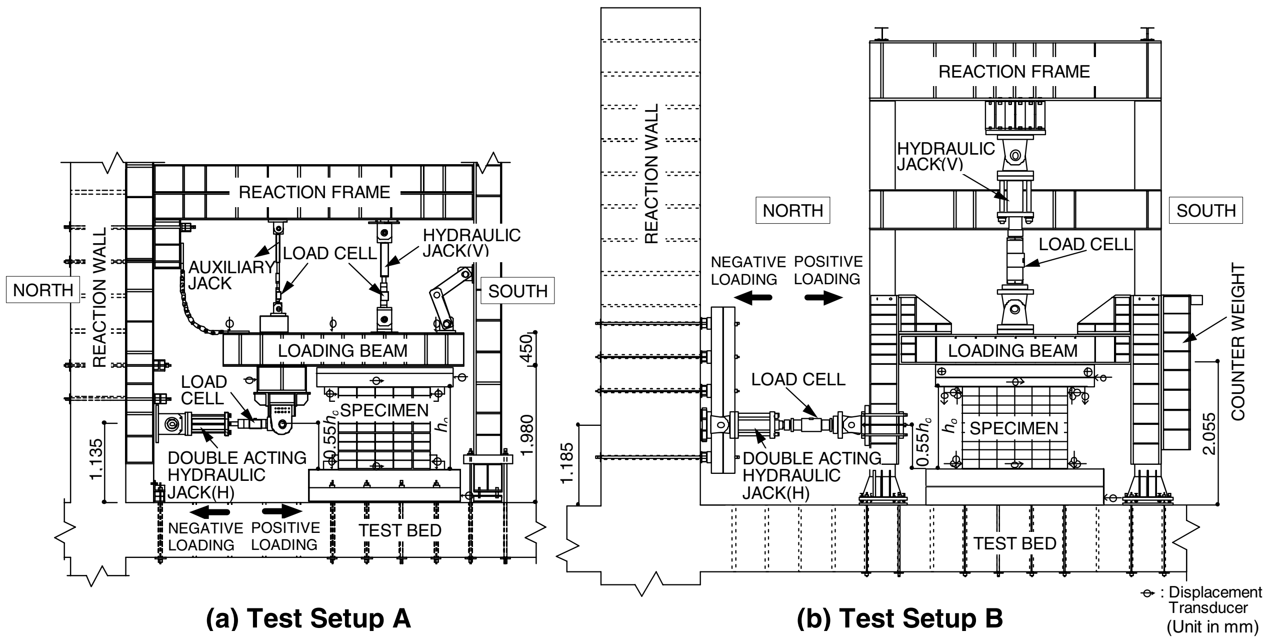

Fig. 6 Test Setup

height (h_o) of the wall panel measured from the bottom of wall. The measuring instruments such as displacement transducers and strain gauges were installed at the specified locations to measure the displacements and stains in reinforcing steel bars and wall surfaces. In addition, in order to measure the flexural, shear and sliding deformation components of the walls, the vertical, horizontal and diagonal displacements in each measuring segment on the East wall surface, where the wall was divided into four measuring segments along the vertical direction, were measured by high sensitivity displacement transducers (Kikuchi [3]).

TEST RESULTS

Typical examples of complete hysteresis loops between the applied lateral force (Q) versus story-drift (R) relations obtained from the tests are shown in Figs. 7(a) through (f) together with the crack and strain information, where the story-drift (R) is defined as an interstory displacement divided by the story-height of the specimen. Ultimate lateral strengths of all the test specimens (Q_{max}) determined from the Q-R hysteresis loops are shown in Table 4 together with the predicted ultimate flexural, shear and sliding strengths (Q_{mu1}, Q_{mu2}, Q_{su}, Q_{sl}), which are determined by the subsequent Equations (3), (4), (5) and (6), respectively. In addition, Table 4 shows the predicted and observed failure modes of all the specimens. As shown in Fig. 7 and Table 4, the observed failure modes can be classified into five different types; <F>: **f**lexural failure, <F_y→S>: **s**hear failure after **y**ield in **f**lexural rebar, <S>: **s**hear failure, <F_y→SL>: **sl**iding failure after **y**ield in **f**lexural rebar, and <SL>: **sl**iding failure.

General observations for the specimens with each failure mode can be summarized as follows:

<F>: The specimens developed their ultimate strengths in flexural failure mode first, and then lateral load-carrying capacity gradually decreased due to the buckling of flexural rebars provided at the wall-edges which occurred at large deformation range (Fig. 7(a)).

<F_y→S>: The specimens failed in brittle shear failure mode after initial yielding in flexural rebars (Fig. 7(b)).

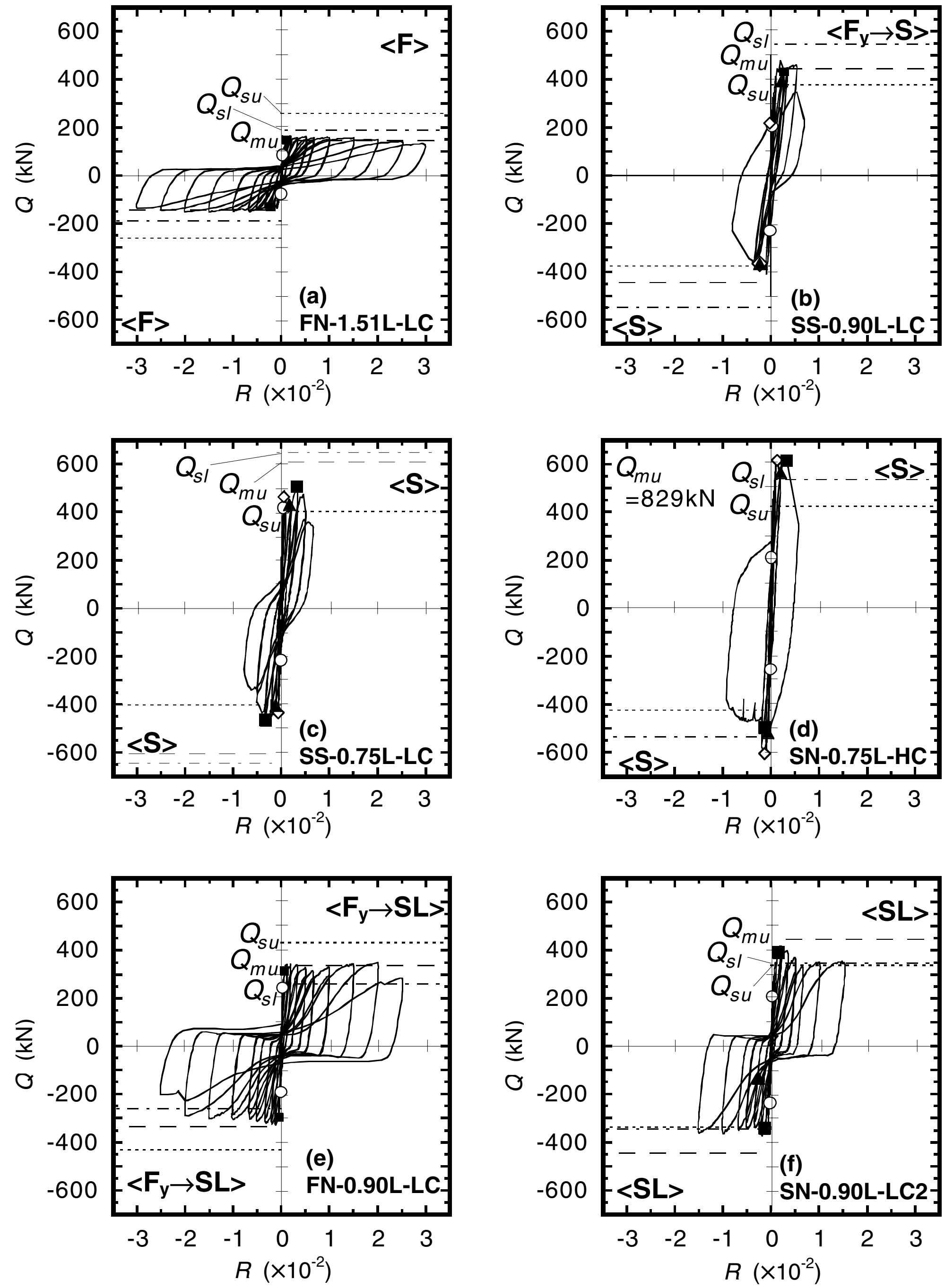

○ : Initial flexural crack, ◇ : Initial shear crack, ■ : Initial yield* in flexural rebars, ▲ : Initial yield* in horizontal rebars

* : Yield in tension rebar

Fig. 7 *Q-R* hysteresis obtained from test

<S>: The specimens failed in brittle shear failure mode without developing their ultimate flexural strengths. Shear cracks extended in diagonal direction and rapid deterioration in lateral load-carrying capacity occurred (Figs. 7(b), (c) and (d)).

<F_y→SL>: The specimens developed almost their ultimate flexural strengths and then sliding displacement between the bottom of wall and the foundation beam gradually increased. However, remarkable deterioration in lateral load-carrying capacity was not observed until the flexural rebars were

Table 4 Predicted and observed initial stiffness, ultimate strengths and failure mode

Specimens		Test Results						Theoretical Prediction						
		$_{test}K_e$ *1 (MN/cm)	Q_{max} *2 (kN)	$\overline{\tau}_{max}$ *2 (MPa)	R_{max} *2 ($\times 10^{-2}$)	R_u *3 ($\times 10^{-2}$)	Observed Failure Mode *4	$_{cal}K_{e1}$ *1 (MN/cm)	$_{cal}K_{e2}$ *1 (MN/cm)	Q_{mu1} *5 (kN)	Q_{mu2} *5 (kN)	Q_{su} *5 (kN)	Q_{sl} *5 (kN)	Predicted Failure Mode *4
FN-1.51L-LC	P *6	2.1	162	1.54	0.51	2.93<	F	4.3	2.8	145	144	259	188	F
	N *6	2.6	152	1.45	0.66	3.00<								
FS-1.51L-LC	P	1.7	171	1.62	0.51	1.86	F	4.4	2.8	145	144	254	275	F
	N	1.8	165	1.56	1.00	1.79								
FN-1.13L-LC	P	4.0	251	1.78	0.20	2.71	$F_y \rightarrow$ SL	7.0	4.3	231	237	332	224	F or SL
	N	9.5	247	1.75	0.67	3.00<								
FS-1.13L-LC	P	3.8	256	1.82	0.20	1.86	F	7.7	4.8	231	237	342	341	F
	N	24.9	258	1.83	0.21	1.22								
FN-0.90L-LC	P	5.4	341	1.93	0.20	2.51<	$F_y \rightarrow$ SL	10.8	6.8	336	350	434	261	SL
	N	8.7	327	1.85	0.13	2.16								
FS-0.90L-LC	P	5.0	376	2.13	0.21	0.95	$F_y \rightarrow$ SL	10.7	6.7	336	350	420	463	F
	N	166.4	366	2.08	0.10	1.07								
SN-1.51L-LC	P	1.7	216	2.05	0.34	0.97	$F_y \rightarrow$ S	4.4	2.8	210	209	219	273	S or F
	N	1.7	198	1.88	0.20	0.63								
SN-1.13L-LC	P	5.5	330	2.34	0.21	0.40	S	7.9	5.0	319	326	311	309	S or F or SL
	N	3.6	303	2.15	0.20	0.42								
SN-0.90L-0	P	3.7	284	1.61	0.19	0.48	SL	10.1	6.4	321	335	334	248	SL
	N	6.9	250	1.42	0.10	0.31								
SN-0.90L-LC	P	7.5	452	2.56	0.33	0.67<	$F_y \rightarrow$ SL	10.5	6.7	446	464	361	345	SL
	N	6.9	387	2.19	0.21	0.68	SL							
SN-0.90L-LC2	P	4.7	416	2.36	0.21	0.65	$F_y \rightarrow$ SL	9.9	6.3	446	465	339	345	S or SL
	N	3.1	374	2.12	0.19	1.50<								
SN-0.90L-HC	P	4.0	506	2.87	0.20	0.42	$F_y \rightarrow$ S	9.9	6.3	603	627	356	466	S
	N	7.5	490	2.78	0.14	0.80	S							
SS-0.90L-0	P	4.6	346	1.96	0.20	0.69	S	10.6	6.7	321	335	349	451	F
	N	12.2	342	1.94	0.20	0.50								
SS-0.90L-LC	P	6.8	476	2.70	0.20	0.58	$F_y \rightarrow$ S	11.2	7.1	446	464	378	548	S
	N	6.8	413	2.34	0.10	0.48	S							
SS-0.90L-LC2	P	5.3	436	2.47	0.20	0.37	S	9.9	6.3	446	465	339	548	S
	N	32.6	462	2.62	0.19	0.37								
SN-0.75L-0	P	5.9	307	1.45	0.12	1.45	SL	12.7	8.1	423	445	388	273	SL
	N	4.3	294	1.39	0.10	1.10								
SN-0.75L-LC	P	8.5	495	2.34	0.13	1.11	SL	12.8	8.2	603	635	402	389	SL
	N	42.7	511	2.41	0.48	0.70	$F_y \rightarrow$ S							
SN-0.75L-HC	P	11.1	629	2.97	0.29	0.41	S	13.0	8.3	829	873	425	534	S
	N	14.9	606	2.86	0.14	0.56								
SS-0.75L-LC	P	6.6	506	2.39	0.32	0.52	$F_y \rightarrow$ S	12.7	8.1	603	635	404	649	S
	N	11.1	479	2.26	0.32	0.53	S							

[Remarks] *1 Initial stiffness obtained from the experiment ($_{test}K_e$) and calculated initial stiffness ($_{cal}K_{e1}$, $_{cal}K_{e2}$).
*2 Ultimate lateral strength (Q_{max}), maximum average shear stress ($\overline{\tau}_{max}=Q_{max}/tl$) and story-drift ($R_{max}$) at the ultimate strength
*3 Limit story-drift (R_u), which is defined as story-drift corresponding to lateral force when lateral load-carrying capacity in *Q-R* envelope curve decreased to 80% of the ultimate lateral strength.
*4 F : Flexural failure mode, S : Shear failure mode, SL : Sliding failure mode,
$F_y \rightarrow$ S : Shear failure mode after flexural yield, $F_y \rightarrow$ SL : Sliding failure mode after flexural yield.
*5 Theoretical ultimate strengths in flexural failure mode (Q_{mu1}, Q_{mu2}), shear failure mode (Q_{su}) and sliding failure mode (Q_{sl})
*6 P : Positive loading, N : Negative loading (see Figure 6).

buckled and pushed out their cover concrete. Their lateral sliding displacements became to be approximately 50 to 60% of total displacement at the end of test (Fig. 7(e)).

<SL>: The specimens failed due to sliding along the bottom of wall. With the increase of story-drift, the ratio of sliding displacement to total displacement became to be larger and reached approximately 70 to 80% at the end of test (Fig. 7(f)).

DISCUSSIONS ON EVALUATION OF SEISMIC CAPACITY

Based on the results of the experiments in the present paper and the Reference (Kikuchi [4]), the seismic capacity of the grouted masonry walls are discussed below. In the experiments presented in the Reference [4], a total of 12 grouted masonry wall specimens were tested in Oita University. Table 5 shows a list of the specimens together with representative test results and predicted values. The test specimens are classified into two series, H-series and L-series, depending on the shear-to-span ratio of wall. Thickness of

Table 5 Observed and predicted initial stiffness ultimate strengths and failure mode of the specimens in Reference [4]

Specimens		Shear Span Ratio M/Ql	Vertical Axial Stress σ_0 (MPa)	Test Results						Theoretical Prediction						
				${}_{test}K_e^{*1}$ (MN/cm)	Q_{max}^{*2} (kN)	$\overline{\tau}_{max}^{*2}$ (MPa)	R_{max}^{*2} ($\times 10^{-2}$)	R_u^{*3} ($\times 10^{-2}$)	Observed Failure Mode*4	${}_{cal}K_{e1}^{*1}$ (MN/cm)	${}_{cal}K_{e2}^{*1}$ (MN/cm)	Q_{mu1}^{*5} (kN)	Q_{mu2}^{*5} (kN)	Q_{su}^{*5} (kN)	Q_{sl}^{*5} (kN)	Predicted Failure Mode*4
H2-C22	P*6	2.10	2.16	0.7	158	1.05	0.67	2.62	F	1.3	0.9	174	154	216	568	F
	N*6			0.7	162	1.08	0.67	2.43								
H2-C8	P		0.78	0.5	125	0.83	0.65	1.97<	F	1.2	0.8	130	115	191	423	F
	N			0.3	120	0.80	0.70	2.03<								
H1-C8	P			0.8	129	0.86	0.67	3.33<	F	1.2	0.9	133	118	194	435	F
	N			0.6	123	0.82	0.67	2.02<								
H2-0	P		0.00	0.4	110	0.73	3.33	3.33<	F	1.3	0.9	104	92	191	341	F
	N			0.5	102	0.68	2.00	2.00<								
H2-T6	P		-0.59	0.3	95	0.63	3.33	3.33<	F	1.3	0.9	85	76	184	279	F
	N			0.5	89	0.59	2.01	3.34<								
H2-V	P		-0.59～2.16	0.9	146	0.97	0.47	3.28<	F	1.3	0.9	174	154	216	568	F
	N			0.5	95	0.63	3.36	3.36<				85	76	184	279	
L2-C22	P	0.84	2.16	3.1	342	2.28	0.16	0.49	S	5.8	3.7	437	387	314	568	S
	N			4.9	329	2.19	0.18	0.35								
L2-C8	P		0.78	1.7	308	2.05	0.49	0.70	$F_y \rightarrow S$	5.6	3.6	326	289	291	423	S or F
	N			2.6	287	1.91	0.33	0.77								
L1-C8	P			1.7	335	2.23	0.31	0.55	$F_y \rightarrow S$	6.1	3.9	335	297	313	435	S or F
	N			1.4	303	2.02	0.41	0.51								
L2-0	P		0.00	2.5	242	1.61	0.28	0.47	$F_y \rightarrow S$	6.0	3.8	262	233	297	341	F
	N			2.2	221	1.47	0.23	0.46								
L2-T6	P		-0.59	1.2	203	1.35	0.32	0.65<	F	6.1	3.9	215	190	292	279	F
	N			1.3	180	1.20	0.33	0.55								
L2-V	P		-0.59～2.16	2.5	347	2.31	0.20	0.55	S	6.3	4.0	437	387	314	568	S
	N			4.2	195	1.30	0.33	0.72	$F_y \rightarrow S$			215	190	292	568	F

[Remarks] see the remarks in Table 4.

the wall panel in the test specimens is 190mm, and the clear height (h_0) and length of the wall are 1200mm and 790mm, respectively.

Initial Stiffness

Figs. 8(a) and (b) show relation between initial lateral stiffness (${}_{test}K_e$) of walls in the positive loading and calculated initial stiffness (${}_{cal}K_{e1}$ or ${}_{cal}K_{e2}$). The experimental initial stiffness is the secant modulus at the occurrence of the initial flexural crack in the wall. Difference in these two equations is a deformable height of wall, which is the clear height of wall in Equation (1) and the clear height plus one quarter of the depth of top and bottom beams in Equation (2), respectively.

$$ {}_{cal}K_{e1} = \frac{1}{\dfrac{(y \cdot h_0)^3 + [(1-y) \cdot h_0]^3}{3E_m \cdot I_e} + \dfrac{\kappa \cdot h_0}{G_m \cdot A}} \tag{1} $$

$$ {}_{cal}K_{e2} = \frac{1}{\dfrac{(y \cdot h_0 + 0.25D)^3 + [(1-y) \cdot h_0 + 0.25D]^3}{3E_m \cdot I_e} + \dfrac{\kappa \cdot h_0}{G_m \cdot A}} \tag{2} $$

where,

${}_{cal}K_{e1}$, ${}_{cal}K_{e2}$: initial stiffness of wall (kgf/cm^2)

E_m : Young's modulus of prism (kgf/cm^2), $E_m = 2.1 \times 10^5 \times \left(\dfrac{\gamma}{2.3}\right)^{1.5} \times \sqrt{\dfrac{F_m}{200}}$

γ : weight per unit volume of prism (=2.3t/m^3)

F_m : prism strength (kgf/cm^2)

G_m : shear modulus of elasticity of prism (kgf/cm^2), $G_m = \dfrac{E_m}{2(1+\nu_m)}$

ν_m : Poisson's ratio of prism (=1/6)

I_e : equivalent geometrical moment of inertia considered the flexural rebars of wall (cm^4)

κ : shape factor for shear rigidity, y : inflection point height ratio

D : depth of top and bottom beams (cm) h_0 : clear height of wall (cm)

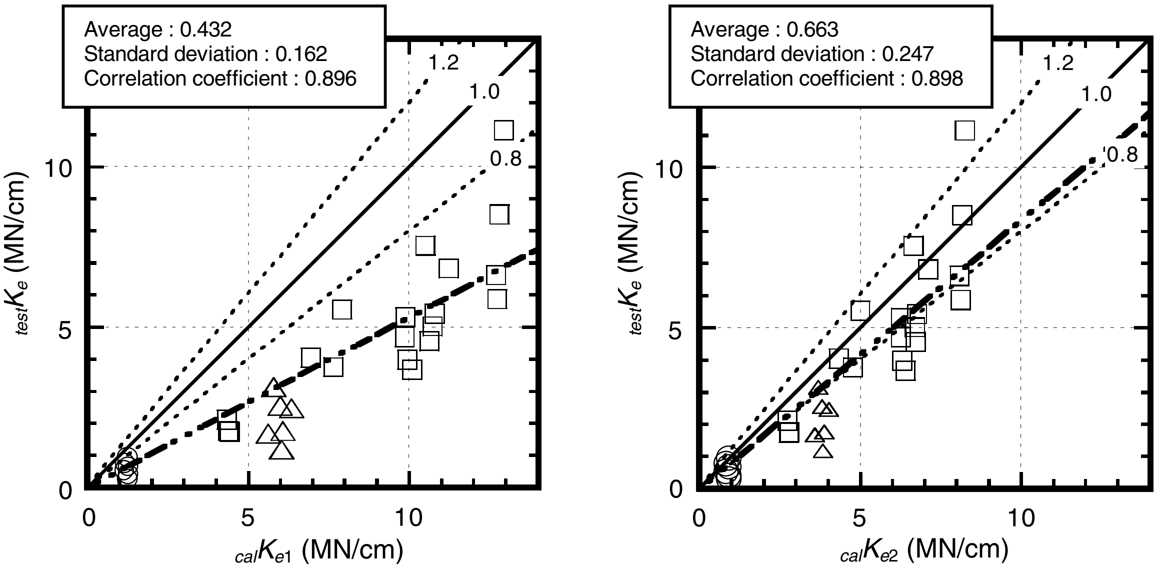

(a) The case of Equation (1) **(b) The case of Equation (2)**

○ : H-series specimens in Reference [4], △ : L-series specimens in Reference [4], □ : Specimens in Table 4

Fig. 8 Relation of initial stiffness obtained from the experiment versus calculated initial stiffness

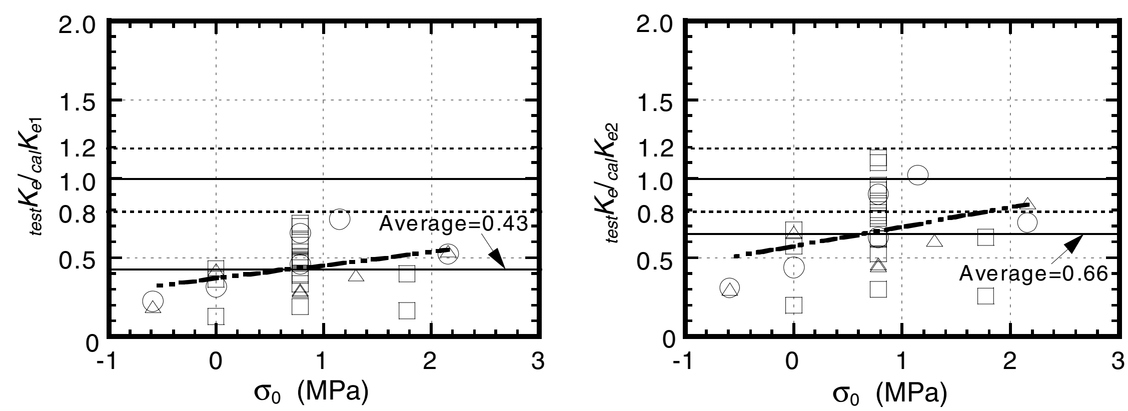

(a) The case of Equation (1) **(b) The case of Equation (2)**

○ : H-series specimens in Reference [4], △ : L-series specimens in Reference [4]
□ : Specimens in Table 4

Fig. 9 Effect of vertical axial stress on initial stiffness

It can be seen from the plots in Fig. 8, the initial stiffness obtained from the experiment is widely scattered even in the specimens with the same aspect ratio and the initial stiffness calculated by Equation (1) is considerably larger than the experimental initial stiffness. On the other hand, the initial stiffness calculated by Equation (2) gives much closer value to the experimental value than Equation (1). However, the specimens plotted within the range of ±20% are only about 30% of all specimens. This result means that it is necessary to improve the estimating equation further.

Figs. 9(a) and (b) show the relation between the ratio of the experimental initial stiffness to the calculated initial stiffness ($_{test}K_e/_{cal}K_{e1}$ or $_{test}K_e/_{cal}K_{e2}$) versus vertical axial stress in the wall (σ_0). As can be seen in these figures, the ratios of initial stiffness have a tendency to become larger as the vertical axial stress becomes larger. Therefore, it is necessary to take into account of the effect of vertical axial stress in order to estimate the initial stiffness of walls accurately.

Ultimate strengths

The ultimate lateral strength (Q_{max}) and failure modes obtained from the experiments are shown in the Tables 4 and 5 together with the calculated ultimate lateral strengths in flexural failure mode (Q_{mu1} and Q_{mu2}), shear failure mode (Q_{su}) and sliding failure mode (Q_{sl}).

The ultimate flexural strength (Q_{mu1}) is calculated by Equation (3), which is based on the existing equations to predict the ultimate flexural strengths of the grouted masonry walls (AIJ [5]). Q_{mu2} is determined by Equation (4), where "l_w :0.9 times the wall length" in Equation (3) is replaced with "l_w': distance between flexural rebars".

$$Q_{mu1} = (a_t \cdot \sigma_y \cdot l_w + 0.5 a_{wv} \cdot \sigma_{wy} \cdot l_w + 0.5 N \cdot l_w) / h_l \qquad (3)$$

$$Q_{mu2} = (a_t \cdot \sigma_y \cdot l_w' + 0.5 a_{wv} \cdot \sigma_{wy} \cdot l_w' + 0.5 N \cdot l_w') / h_l \qquad (4)$$

where,

Q_{mu1}, Q_{mu2} : ultimate flexural strength

a_t : cross-sectional area of flexural reinforcement in tension side

σ_y : yield strength of flexural reinforcement, l_w : 0.9 times wall length

l_w' : distance between flexural rebars, a_{wv} : cross-sectional area of vertical shear reinforcement

σ_{wy} : yield strength of shear reinforcement, N : vertical axial load

h_l : height of the longitudinal axis of lateral forces applied to the specimen, which is measured from the bottom of wall

For the specimens that failed in the flexural failure mode, the ultimate lateral strength obtained from the experiment is compared with the calculated ultimate flexural strength as shown in Figs. 10(a) and (b),

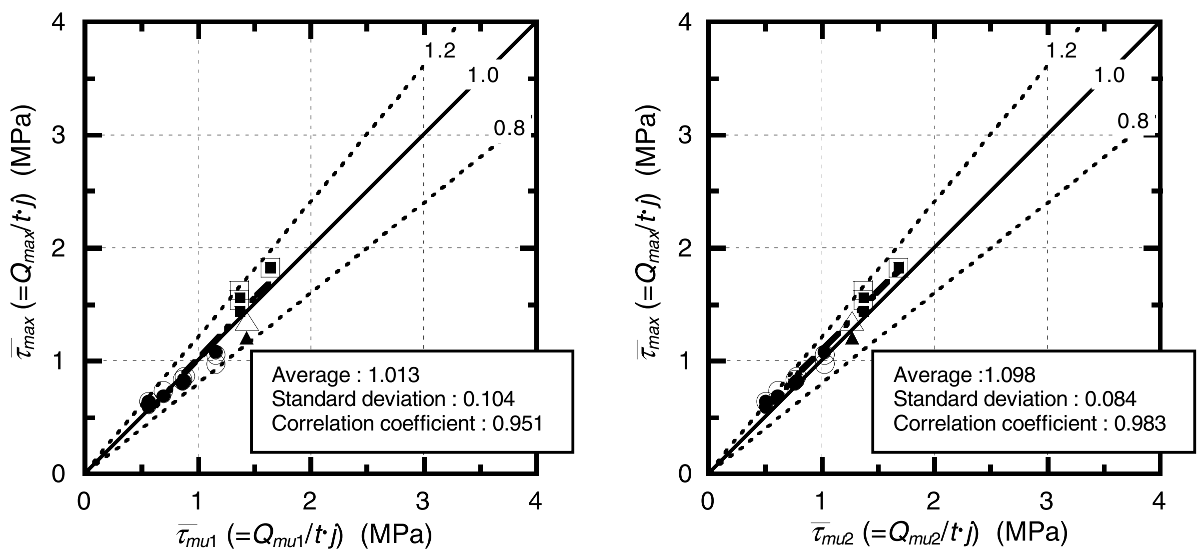

(a) The case of Equation (3) **(b) The case of Equation (4)**

○, ● : H-series specimens in Reference [4], △, ▲ : L-series specimens in Reference [4]

□, ■ : Specimens in Table 4

Negative loading

Positive loading

Fig. 10 Relation between ultimate strength obtained from the experiment versus calculated ultimate flexural strength

where these ultimate strengths (Q_{max}, Q_{mu1} and Q_{mu2}) are expressed as the average shear stresses ($\overline{\tau}_{max}$, $\overline{\tau}_{mu1}$ and $\overline{\tau}_{mu2}$), respectively. The average shear stresses were calculated by dividing the ultimate strengths by the cross-sectional area of the wall ($=t \times l$). It can be understood from these figures that the ultimate flexural strengths can be well predicted within the error of 20% by either Equation (3) or Equation (4). The correlation coefficients of the experimental and calculated values are 0.951 and 0.983 for the case of the Equation (3) and Equation (4), respectively. This means that the Equation (4) is slightly better than the Equation (3) for estimating the ultimate flexural strength.

The ultimate shear strength (Q_{su}) is calculated based on the existing equation to predict lower bound of the ultimate shear strength for the grouted masonry walls (AIJ [5]). This equation is given by Equation (5).

$$Q_{su} = \left\{ \frac{0.053 p_t^{\ 0.23} \left(F_m + 180 \right)}{M / Qd + 0.12} + 2.7 \sqrt{\sigma_{wh} \cdot p_{wh}} + 0.1 \sigma_0 \right\} \cdot t \cdot j \tag{5}$$

where,

Q_{su} : ultimate shear strength (kgf), p_t : flexural reinforcement ratio (in %)
F_m : compressive strength of prism (kgf/cm^2), t : thickness of masonry wall (cm)
M : maximum design bending moment of masonry wall (kgf·cm)
Q : maximum design shear force of masonry wall (kgf)
d : effective length of masonry wall considering the flexural rebars (cm)
p_{wh} : shear reinforcement ratio, σ_{wh} : yield strength of shear reinforcement (kgf/cm^2)
σ_0 : vertical axial stress (kgf/cm^2)
j : distance between compressive and tensile resultants (=7/8d ; cm)

Fig. 11 shows relation between the experimental and calculated ultimate shear strengths of the shear failure specimens. As can be seen from this figure, the experimental values are scattered within 90% to 150% of their calculated values. In order to investigate the effect of vertical axial load applied to the wall

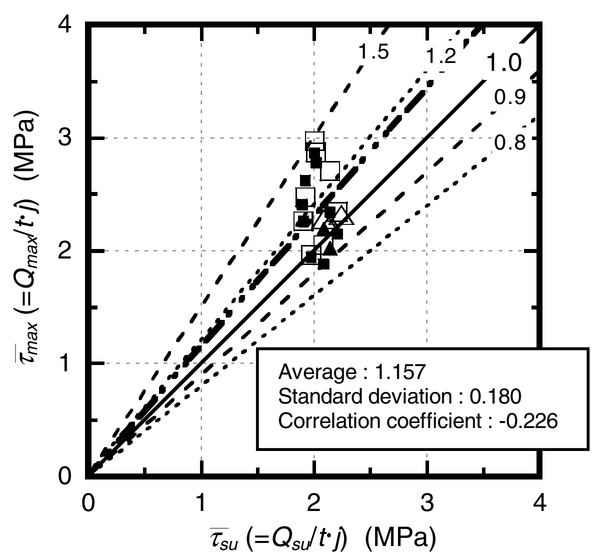

○, ● : H-series specimens in Reference [4], △, ▲ : L-series specimens in Reference [4]
□, ■ : Specimens in Table 4
Negative loading
Positive loading

Fig. 11 Comparison of observed and calculated ultimate shear strengths

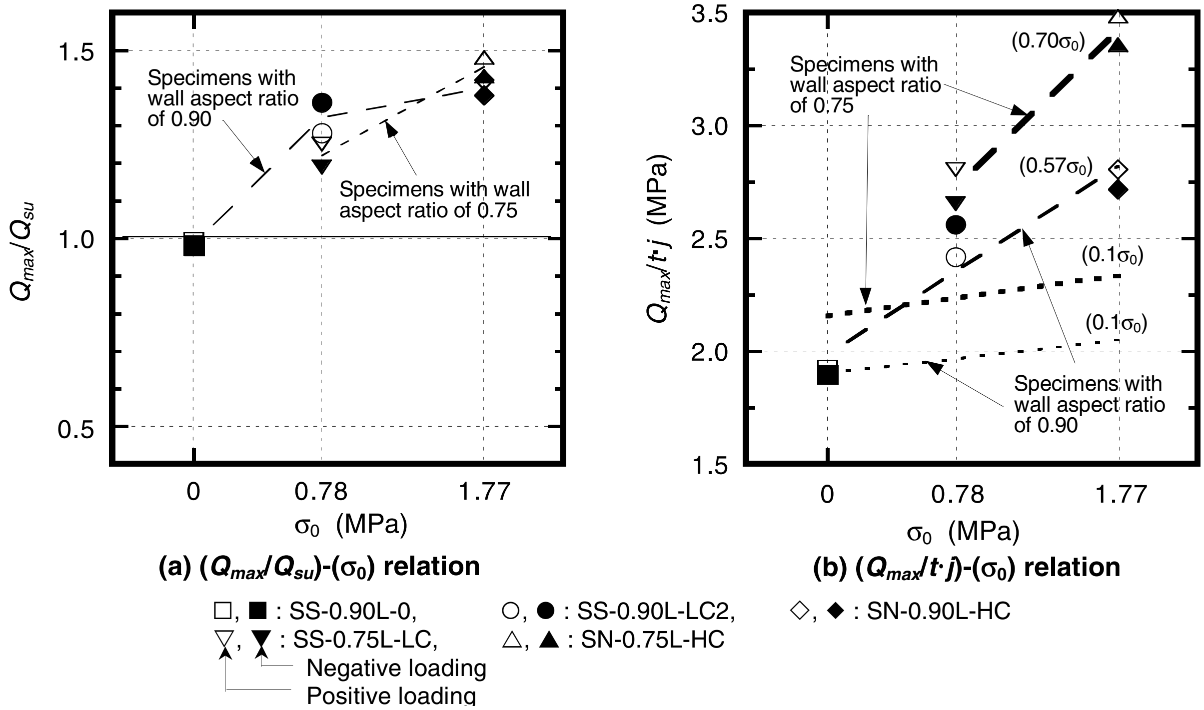

Fig. 12 Effect of vertical axial stress on ultimate shear strength

on the ultimate shear strength, the ratios (Q_{max}/Q_{su}) and ultimate shear stresses ($Q_{max}/t{\cdot}j$) of two types of specimens having the wall aspect ratios of 0.90 and 0.75, which failed in shear failure mode, are plotted against the vertical axial stresses (σ_0) in Figs. 12(a) and (b), respectively. In these figures, the values of (Q_{max}/Q_{su}) and ($Q_{max}/t{\cdot}j$) have a tendency to become larger with the increase of the vertical axial stress. In Fig. 12(b), regression lines for each type of the specimens are given by dashed lines, where increasing factor is 0.57 for the specimens with the aspect ratio of 0.90 and 0.70 for the specimens with the aspect ratio of 0.75. The obtained increasing factor is considerably larger than 0.1, which appears in the third term of Equation (5). This would be one of the main reasons why the observed maximum lateral strengths of the specimens failed in shear failure mode are generally much higher than those of the evaluations given by the Equation (5).

The ultimate sliding strength (Q_{sl}) is calculated by Equation (6), which is based on the existing equation to predict the ultimate sliding strength of the precast reinforced concrete walls (AIJ [6]).

$$Q_{sl} = 0.7\left(a_t \cdot \sigma_y + a_{wv} \cdot \sigma_{wy} + a_d \cdot \sigma_{dy}\right) + 0.7N \tag{6}$$

where,

Q_{sl} : ultimate strength in sliding failure mode

σ_y, σ_{wy}, σ_{dy} : yield strength of flexural, vertical shear and dowel reinforcement, respectively.

a_t ,a_{wv}, a_d : cross-sectional area of flexural, vertical shear and dowel reinforcement, respectively.

N : vertical axial load

In Fig. 13, the ultimate strengths of the specimens, which failed in sliding failure mode, are plotted against the calculated ultimate sliding strength from Equation (6). It can be understood from this figure that the experimental values are 0 to 30% larger than the calculated values. In Figs. 14(a) and (b), the ultimate lateral strength (Q_{max}) obtained from the experiments for two types of specimens having the wall aspect ratios of 0.90 and 0.75, which failed in sliding failure mode, are plotted against the vertical axial load (N).

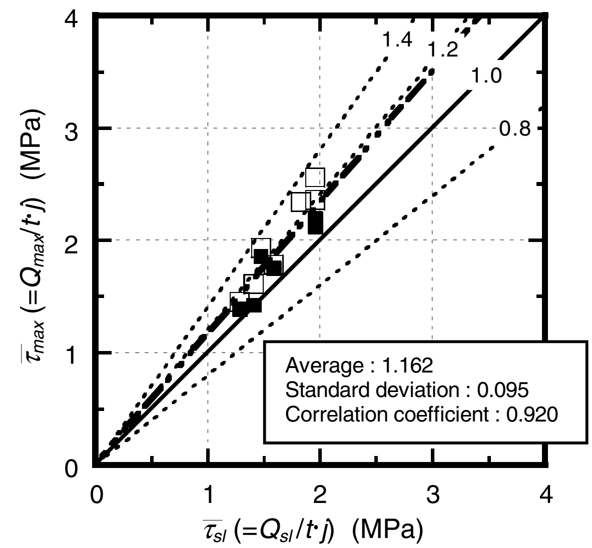

□, ■ : Specimens in Table 4
Negative loading
Positive loading

Fig. 13 Comparison of observed and calculated ultimate sliding strengths

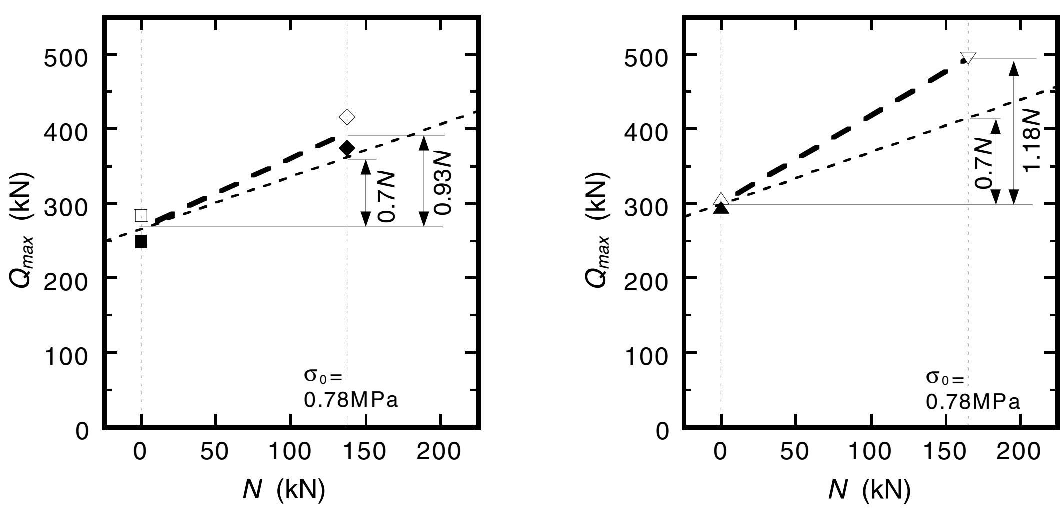

(a) Specimens with wall aspect ratio of 0.90 (b) Specimens with wall aspect ratio of 0.75

□, ■ : SN-0.90L-0, ◇, ◆ : SN-0.90L-LC2, △, ▲ : SN-0.75L-0, ▽ : SN-0.75L-LC
Negative loading
Positive loading

Fig. 14 Effect of vertical axial loads on ultimate sliding strength

Dashed lines in these figures represent the regression lines for the plots of each type of the specimens. In Equation (6), the effect of vertical axial load on the ultimate sliding strength is evaluated as 0.7N. As shown in these figures, however, this effect obtained from the experimental results is 0.93N for the aspect ratio of 0.90 and 1.18N for the aspect ratio of 0.75, which are considerably larger than 0.7N.

Deformation Capacity

Figs. 15(a) through (e) show the (Q/Q_{max})-(R) envelope curves in the positive loading, which are classified by the failure mode. In these figures, the symbols, "◇" and "○", represent the story-drift at the ultimate strength (R_{max}) and the limit story-drift (R_u) of each specimens, respectively. R_u is defined as the story-drift corresponding to the lateral force when the lateral load-carrying capacity in the Q-R envelope curves decreased to 80% of the ultimate strength. As can be seen from Fig. 15(a), in case of the specimens that failed in flexural failure mode (F), the values of R_{max} and R_u are widely scattered because of the effect of vertical axial load applied to the specimens. Except for the tested specimens under zero or tensile vertical axial loads, other specimens developed their ultimate lateral strengths at R=(0.2 to 0.5)$\times 10^{-2}$ and then reached the limit story-drifts more than R=1.9$\times 10^{-2}$ without any rapid deterioration in lateral load-carrying capacity. On the contrary, in case of the specimens that failed in shear failure mode (S and $F_y \rightarrow S$) shown in Figs. 15(b) and (d), R_{max} is R=(0.2 to 0.3) $\times 10^{-2}$ and R_u is R=(0.4 to 1.0) $\times 10^{-2}$. These limit story-drifts are considerably smaller than those of the specimens, which failed in flexure. While, in case of the specimens that failed in sliding failure mode (SL and $F_y \rightarrow SL$) shown in Figs. 15(c) and (e), R_{max} is R=(0.1 to 0.3) $\times 10^{-2}$ and R_u is R=(0.5 to 2.7) $\times 10^{-2}$. For most of the sliding failure specimens, recovery of lateral load-carrying capacity are observed at around R=(0.5 to 0.7) $\times 10^{-2}$.

The specimens strengthened by the dowel rebars except for the specimen FS-0.9L-LC, of which the wall bottom slipped along the horizontal joint at the top of lowest concrete masonry units, did not fail in sliding failure. This fact means that the sliding strengthening by using the dowel rebars is effective to prevent the grouted masonry walls from sliding failure at the bottom of the walls. However, the deformation capacity of the wall with dowel rebars is inferior to the wall without any dowel rebars.

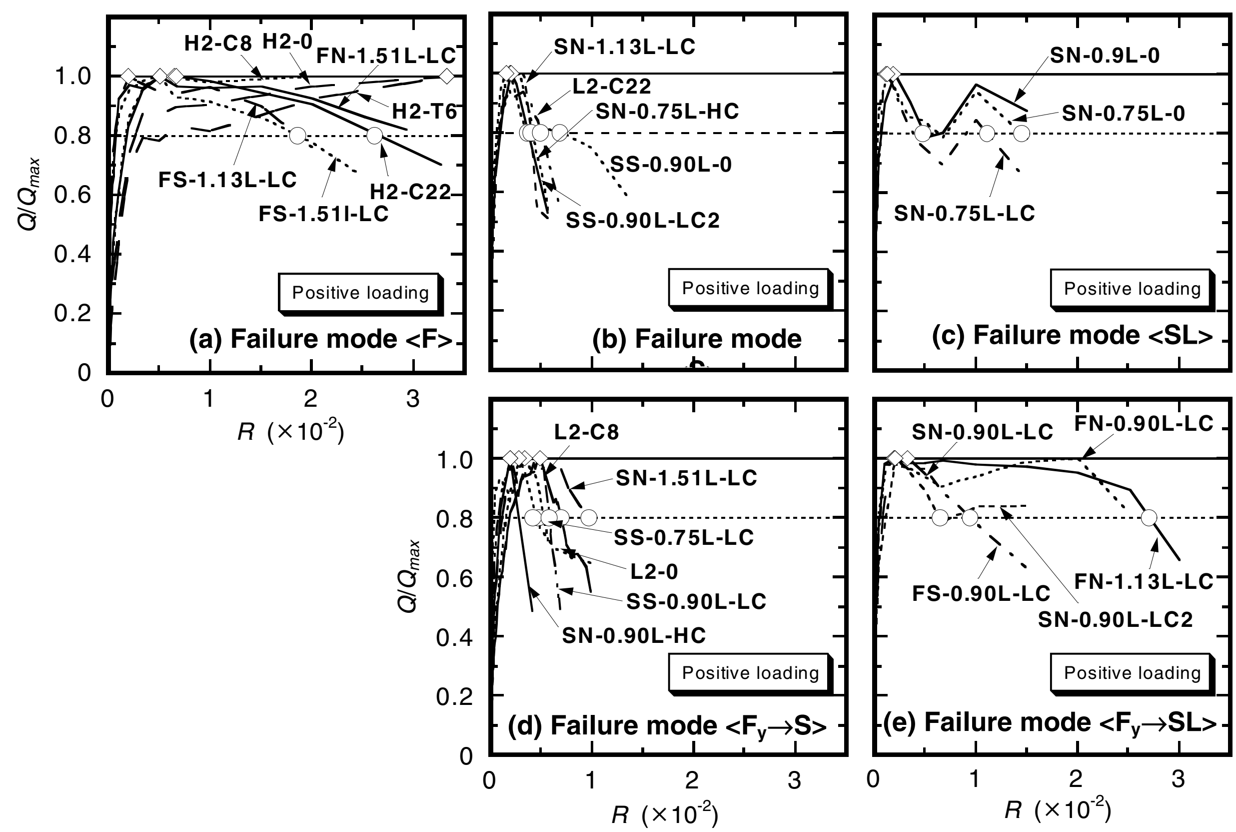

Fig. 15 Envelope curves of Q/Q_{max} – R relation

CONCLUSIONS

Based on the results obtained from the experiments for a total of thirty-one specimens in the present study and Reference [4], the seismic capacity of the reinforced fully-grouted concrete masonry wall were investigated. The obtained conclusions are as follows:

1. The initial stiffness of grouted masonry wall can be roughly estimated by Equation (2), though those obtained from the experimental observation are widely scattered.

2. The ultimate flexural strength of grouted masonry wall can be well evaluated by using the existing Equation (3) or modified Equation (4).

3. The accuracy in estimating the ultimate shear and sliding strengths of grouted masonry wall by the existing equations varies widely. This accuracy can be improved by modifying the term related to vertical axial load in those equations.

4. The sliding strengthening by using dowel rebars is effective to prevent the grouted masonry walls from sliding failure at the bottom of the walls.

ACKNOWLEDGEMENT

The authors wish to express many thanks to Mr. M. Kuroki and Mr. T. Hiramatsu of Oita University for their cooperation during the experiments.

REFERENCES

1. Bruneau, M. and Yoshimura, K., “Damage to masonry buildings caused by the 1995 Hyogo-ken Nanbu (Kobe, Japan) Earthquake,” Canadian Journal of Civil Engineering, Vol. 23, No. 3, 1996, pp.797-807.
2. Architectural Institute of Japan (AIJ), AIJ Standards for Structural Design of Masonry Structures (1997), in Japanese.
3. Kikuchi, K., Yoshimura, K., Tanaka, A. and Yoshida K., “Effect of wall aspect ratio on seismic behavior of reinforced fully grouted concrete masonry walls,” Proceedings of the 9th North American Masonry Conference, Clemson, USA, Vol. 1, 2003, pp.214-225.
4. Kikuchi, K., Yoshimura, K., Kanema, T. and Tanaka, A., “Effect of vertical axial loads on seismic behavior of grouted masonry walls,” Proceedings of the 11th International Brick/Block Masonry Conference, Shanghai, China, Vol. 1, 1997, pp.595-604.
5. Architectural Institute of Japan (AIJ), Ultimate Strength and Deformation Capacity of Buildings in Seismic Design (1990), pp.605-606, in Japanese.
6. Architectural Institute of Japan (AIJ), AIJ Standards for Structural Design of Precast Reinforced Concrete Boxed-Wall Structures (1984), p.78, in Japanese.